APS European Society for Paediatric Research Society for Pediatric Research

BASIC SCIENCE ARTICLE

Check for updates

Intraventricular hemorrhage induces inflammatory brain damage with blood–brain barrier dysfunction in immature rats

Aarón Del Pozo[1], María Villa[1], Carlos Vargas[1], David Castejón[2], M. Encarnación Fernández-Valle[2], Ana Gutiérrez-Rodríguez[1] and José Martínez-Orgado[1,3]✉

BACKGROUND: We aimed to characterize a preclinical model of intraventricular hemorrhage-induced brain damage (IVH-BD) in extremely low birth weight newborns (ELBWN), to identify potential therapeutic targets based on its pathophysiology.
METHODS: IVH was induced in 1-day-old (P1) Wistar rats by left periventricular injection of clostridium collagenase (PVCC). At P6, P14, and P45 IVH-BD (area of damage, motor and cognitive deficits, Lactate/*N*-acetylaspartate ratio), white matter injury (WMI: ipsilateral hemisphere and corpus callosum atrophy, oligodendroglial population and myelin basic protein signal reduction), blood–brain barrier (BBB) dysfunction (occludin and Mfsd2a expression, Gadolinium leakage) and inflammation (TNFα, TLR4, NFkB, and MMP9 expression; immune cell infiltration), excitotoxicity (Glutamate/*N*-acetylaspartate), and oxidative stress (protein nitrosylation) were assessed. Sham animals were similarly studied.
RESULTS: IVH-BD leads to long-term WMI, resulting in motor and cognitive impairment, thus reproducing IVH-BD features in ELBWN. BBB dysfunction with increased permeability was observed at P6 and P14, coincident with an increased inflammatory response with TLR4 overexpression, increased TNFα production, and increased immune cell infiltration, as well as increased excitotoxicity and oxidative stress.
CONCLUSIONS: This model reproduced some key hallmarks of IVH-BD in ELBWN. Inflammation associated with BBB dysfunction appears as relevant therapeutic target to prevent IVH-BD-induced WMI.

Pediatric Research (2023) 93:78–88; https://doi.org/10.1038/s41390-022-02062-3

IMPACT:

- Paraventricular injection of clostridium collagenase (PVCC) to 1-day-old Wistar rats uniquely reproduced the neuroimaging, histologic and functional characteristics of intraventricular hemorrhage-induced brain damage (IVH-BD) in extremely low birth weight newborns (ELBWN).
- PVCC-induced IVH triggered a prolonged inflammatory response associated with blood–brain barrier increased permeability, which in turn facilitates the infiltration of inflammatory cells.
- Thus, PVCC led to white matter injury (WMI) resulting in long-term motor and cognitive impairment.
- This model offers a valuable tool to obtain further insight into the mechanisms of IVH-BD in ELBWN and proposes some key therapeutic targets.

INTRODUCTION

Intraventricular hemorrhage (IVH) is diagnosed in about 25% of extremely low birth weight (under 1500 g) preterm newborns (ELBWN),[1,2] representing a major risk factor for developmental problems, with 50–75% of ELBWN with severe IVH developing severe sequelae as post-hemorrhagic hydrocephalus and/or cerebral palsy (CP) due to white matter injury (WMI).[1] Concern over the long-term effects of IVH is not limited to severe IVH. Even mild or moderate IVH increases the risk for developmental disturbances in ELBWN twofold.[3] However, there is no current treatment for IVH in those babies.[4]

Neuroinflammation, together with excitotoxicity and oxidative stress, is thought to play a key role in IVH pathophysiology.[4,5] In addition to direct brain damage, inflammation leads to increased permeability of the blood–brain barrier (BBB), which is the main component of post-IVH brain damage.[6] However, although anti-inflammatory treatments such as prenatal steroids[7] or prophylactic indomethacin[8] reduce the incidence of IVH in ELBWN, their effects on post-hemorrhagic hydrocephalus or CP are controversial and the burden of the related side effects is a cause for concern.[7,8] Therefore, further research on therapeutic strategies for this condition is warranted.

Preclinical murine models of brain pathology have been widely used because of their feasibility, reproducibility, and availability for long-term outcome studies.[4,6,9] Among the murine models, periventricular injection of clostridium collagenase (PVCC),

[1]Biomedical Research Foundation, Hospital Clínico San Carlos – IdISSC, 28040 Madrid, Spain. [2]ICTS Bioimagen Complutense (BiolmaC), Complutense University, 28040 Madrid, Spain. [3]Department of Neonatology, Hospital Clínico San Carlos – IdISSC, 28040 Madrid, Spain. ✉email: jose.martinezo@salud.madrid.org

Received: 1 December 2021 Revised: 18 March 2022 Accepted: 23 March 2022
Published online: 15 April 2022

originally described for adult rodents[10] and then adapted to neonatal rats,[11] aims to reproduce a major component of IVH such as spontaneous rupture of ganglionic eminence vessels, resulting in intraventricular bleeding.[1] This approach results in neonatal rats in severe injury with long-term impairment on brain growth, ventricular enlargement, and persistent neurobehavioral impairment without spontaneous recovery,[6,11] similar to that observed in the clinical setting.[12] In this model, a long-lasting brain inflammatory reaction with activation of microglia in the perilesional area and cortex[13] and increased BBB permeability[14,15] has been reported. However, the collagenase model has been mostly performed on P5-P7 rats,[11,15] which have a developmental brain stage similar to that of a 34–36-week-old human newborn,[16] with very few reports of collagenase-injecting models in more immature rats.[17]

In this work, we aimed to study the role of inflammation in IVH-induced brain damage using a model that more closely reproduces IVH pathophysiology in ELBWN by PVCC in P1 rats, which is at a developmental stage comparable to 24-to-25-week-old preterm babies.[16]

METHODS

Animals

Timed pregnant Wistar rats obtained from a qualified supplier (Charles River, Barcelona, Spain) were housed with free access to food and water. On postnatal day 1 (P1), pups were blindly assigned to sham (SHM) or collagenase-infusion groups (IVH). All groups were evenly divided, and sex was balanced within each litter. The sample size for each experiment is presented in Supplementary Material (Table S1). All procedures complied with European and Spanish regulations (2010/63/EU and RD 53/2013) and were approved by the San Carlos University Hospital Animal Welfare Ethics Committee (Madrid, Spain). All experimental procedures were designed and performed by personnel qualified in Laboratory Animal Science, according to FELASA recommendations to reduce animal stress and enhance animal welfare. A major effort was made to minimize suffering and reduce the number of animals used.

IVH induction

The experimental model was based on that of Lekic et al.[11] After randomization, rat pups from the IVH group (IVH) were gently anesthetized with 5% sevoflurane (5% induction, 3% maintenance) and placed prone in a stereotaxic frame (VWR International Ltd, Radnor, PA) coupled to a gas anesthesia mask (VWR International Ltd). Stereotactic coordinates were determined using Bregma as a reference: anterior–posterior, A–P = + 0.5 mm; medial–lateral, M–L = +1.3 mm; dorso–ventral, D–V = −2.3 mm. Then, 0.5 µL containing 0.2 U of clostridial collagenase VII-S (Sigma-Aldrich, St Louis, MO) and sterile PBS was injected for three minutes into the left germinal matrix using a 33-gauge Hamilton syringe (HAMI65460-03, Hamilton Company, Reno, NV) coupled to a syringe holder (6860, VWR International Ltd). Collagenase dose was selected after previous experiments demonstrating no damage with 0.1 U and massive hematoma with 0.3 U. The needle remained in place for an additional 9 min after injection to prevent back-leakage. The entire procedure lasted 20 min on average. Upon recovering from anesthesia, the animals were returned to their dams. Sham animals did not receive any surgery.

At the end of the experiment, rats were sacrificed by lethal injection of thiopental sodium and fentanyl citrate. Some rats were transcardially perfused with cold paraformaldehyde (4%) and sodium chloride (0.9%) and their brains were removed and placed in paraformaldehyde 4% for histologic studies. Other rats were perfused with sodium chloride alone and their brains were removed and snap frozen to then be stored at −80 °C for spectroscopy or biochemical studies.

MRI studies

MRI was performed in P6 and P45 at the BioImaC (Universidad Complutense, Madrid, Spain), a node of the ICTS ReDiB, using 1 Tesla benchtop MRI scanner [Icon (1T-MRI); Bruker BioSpin GmbH, Ettlingen, Germany]. Technical specifications are provided in Supplementary Material. In each slice from T2WI, hyperintense and hypointense areas -those with density outside ±1 SD of mean density as measured using ImageJ 1.34 s software (NIH, Bethesda)- corresponding to ventricular bleeding or periventricular edema or hematoma areas were manually delineated using ImageJ. The resulting area was referred to as the whole-brain area in the corresponding slice and then summed to yield the entire volume of the lesion. The corpus callosum (CoCa) area was calculated using the same software. After determining that the slice corresponding to the 21 plate of Paxino's atlas[18] was the most representative of CoCa area reduction, that slice was the one selected for the analysis.

To assess BBB permeability, 0.2 mL/kg of a solution of 279.3 mg/mL of the Gadolinium (Gd)-based contrast agent Gadoteridol (ProHance, Bracco International, The Netherlands) was administered i.v. through the tail vein at P6, P14, and P45. Coronal and axial 2D T1-weighted MRI (T1WI) were obtained before and 5, 20, and 60 min following Gd administration to determine the concentration and the area of extravasated Gd in brain tissue.

Neurobehavioral studies

A set of sensorimotor and cognitive tests were performed at P15 or P45.[19] All tests were video recorded to be assessed by three different examiners blinded to the experimental group. In short, the tests performed were:

At P15:

Inverse geotaxis (coordination) time required to turn 180° after being placed downwards on a ramp tilted at 45°.

Grip test (strength) grasp reflex score after leaning a thin rod against each paw palm.

At P45:

Beam test (coordination) time to cross and foot faults by each hind limb whilst crossing a 1 m long beam.

Cylinder rearing test (CRT; hemiparesis). The rat was placed in a methacrylate transparent cylinder (20 cm diameter and 30 cm height). Initial forepaw preference (left, right, or both) was counted during a 3 min trial (minimum of 4 wall contacts).

Novel object recognition (NOR; working memory) time spent on exploration of the familiar and the novel object after being allowed to explore a methacrylate box (40 × 40 × 35 cm) containing two identical objects and then returned to the box replacing one of the original objects with a new object.

Histologic studies

Paraffin-embedded coronal sections (4 µm thick) were obtained at a level corresponding to plate 21 of the Paxinos and Watson Atlas.[18] To assess PVCC-induced brain damage hematoxylin-eosin studies were performed at P6. Microphotographs from three areas corresponding to the ipsilateral striatal area were obtained.

To assess long-term effects on myelination, immunohistochemistry studies were performed at P6, P14, and P45 in the ipsilateral External Capsule as previously reported.[19,20] Tissue was incubated overnight at room temperature with Olig-2 (1:100; R&D Systems, Minneapolis, MN), to label immature oligodendrocytes (OL) and GST-π (1:100; Abcam, UK) to label mature OL; at P45 Myelin Basic Protein (MBP) antibodies (1:600; Merck KGaA, Darmstadt, Germany) were used too. To assess the microglial and macrophage population in the ipsilateral Striatum at P14 and P45, tissue was incubated with Iba-1 (1:400, Wako, VA) as reported.[19] The corresponding Alexa-Fluor conjugated secondary antibody (1:200; Life Technologies, Spain) was incubated for two hours at 37 °C. Microphotographs from three areas (250 × 250 µm) at the ipsilateral and contralateral External Capsule or ipsilateral Striatum were obtained using a Leica TCS SP5 confocal microscope system (Leica, Wetzlar, Germany). MBP signal intensity was determined with the LEICA LASF Software (Leica Microsystems, Germany) and expressed as a ratio of ipsilateral MBP intensity vs. contralateral intensity (1). Both histologic studies were performed by a researcher blinded to the experimental group.

Biochemical studies

Western blot analysis was performed on brain samples containing 20 µg of total protein at P6, P14, and P45 as reported elsewhere[21] and detailed in Supplementary Material. To assess neuroinflammation, the expression of Toll-like receptor 4 (TLR4) was determined and that of TNFa and NFkB using TLR4 antibodies (1:100; Santa Cruz, CA) and the corresponding antibodies (1:100; R&D Systems, MN), respectively. To assess BBB integrity, expression of occludin, metallopeptidase 9 (MMP9), and major facilitator

superfamily domain-containing protein 2A (Mfsd2a) were determined using the corresponding antibodies (all 1:100; Santa Cruz, CA). Protein levels were expressed as protein measured/β-actin ratio.

To assess oxidative stress, protein nitrosylation using Oxyblot was quantified using a detection kit (Oxyblot, Millipore Iberica; Madrid, Spain) according to the manufacturer's protocol. Results were expressed as OxyBlot/Total Lane Protein ratio.

Spectroscopy studies

Proton nuclear magnetic resonance spectroscopy (^{1}H-NMR) was performed at P6 as reported elsewhere[21,22] on frozen samples from the striatal area at the IPUCM. A Bruker AVIII500HD 11.7 T spectrometer (Bruker BioSpin, Karlsruhe, Germany) was used, equipped with a 4 mm triple channel 1H/13C/31P High-Resolution Magic Angle Spinning resonance probe to calculate several ratios, including lactate/*N*-acytylaspartate (Lac/NAA. brain tissue injury) and glutamate/*N*-acytylaspartate (Glu/NAA, excitotoxicity) ratios.

Flow cytometry assay

Single-cell suspensions were obtained from brain samples at P6, P14, and P45. A detailed description of flow cytometry methodology is provided as Supplementary Material. In short, to determine the microglia/macrophage population cells were incubated with fluorescent antibodies CD11b-APC (BD, San Diego) and CD45-PE-Cy (BD, San Diego), NOS2-Alexa fluor (Santa Cruz, Texas), Arginase PE (RD, Minneapolis), O4 PE (Milteny Biotec, Spain), O1 efluor 600 (Invitrogen, CA), and MOG Alexa fluor 488 (Santa Cruz, CA). Samples were analyzed on a flow cytometer Gallios (Beckmann Coulter, Brea, CA) and data were analyzed using the Kaluza software (Beckmann Coulter, Brea, CA).

Gating on CD45 and CD11b revealed two distinct CD11b+ populations, a $CD45^{low}$ population, representing resident microglial cells, and a $CD45^{high}$ population, representing activated microglia/macrophages and infiltrating leukocytes.[23] Finally, CD11b+CD45+ population was identified as M1 (iNOS) or M2 (Arginase) phenotype using iNOS/Arginase ratio.[23,24] To study oligodendroglial (OL) cells, the procedure was similar, but in this case, samples were obtained at P14 a cell labeled with O4 as a marker of pre-OL, O1 as a marker of immature OL, and MOG as a maker of mature pre-myelinating OL. That time point was selected because in Wistar rat brain at P14 the density of the different developmental stages of OL lineage is high enough to be able to assess the effects of brain injury.[25]

Statistical analysis

Data were analyzed with a statistical software package (GraphPad Prism 9; GraphPad Software, San Diego, CA). After assessing the normality of data distribution using the D'Agostino-Pearson test, data revealing a normal distribution were displayed as mean ± SEM and compared using the Student's *t* test for paired analysis. Data showing a non-normal distribution were displayed as median (IQR) and compared using the Mann-Whitney test for paired analysis. The distribution of qualitative parameters was studied using the X^2 test. A value of $P < 0.05$ was considered statistically significant.

RESULTS

Rats from both groups were similar in terms of sex distribution, post-procedure mortality, and weight at the procedure. However, mean daily weight gain over follow-up was lower in IVH than in SHM rats ($P = 0.01$). All data are presented in Table 1.

Table 1. General data.

	SHM	IVH
Male/female (*n*)	24/18	25/32
Weight at the procedure (g)	6.3 (0.1)	6.5 (0.1)
Weight at the end (g)	176 (5)	154 (5)*
Daily weight gain (g/day)	5.7 (0.1)	4.8 (0.1)*
Death after the procedure (*n*)	2/42	10/57

Data are mean (SEM).
SHM sham, *IVH* intraventricular hemorrhage.
*Student's t test: for "weight at the end" and "daily weight gain", P = 0.01; for "weight at procedure", P = 0.89; for "male/female proportion", $X^2 = 4.7$, P = 0.45; and for death after the procedure, $X^2 = 3.7$, P = 0.1.

IVH induction

PVCC led to GM hemorrhage further extended into ventricles leading in some cases to ventricular dilation, which was apparent five days after the procedure (Fig. 1a–e). The relative volume of damage, expressed as a percentage of total brain volume, remained stable over time, with similar values observed at P6 and P45 in the same animals (Fig. 1c).

Perilesional brain tissue damage was assessed at P6 in the adjacent striatal area using hematoxylin–eosin staining, revealing the presence of a cluster of red blood cells but not hematoma as well as severe decrease of cell density together with neuropil damage (Fig. S1 in Supplementary Material). In the same area, ^{1}H-NMR studies (Fig. 1f–i) demonstrated that the Lac/NAA ratio was increased in the IVH rat brain as compared to SHM (Fig. 1g).

Functional consequences of IVH

IVH led to impaired coordination with poorer performance in the geotaxis test at P14 (Fig. 2a). Moreover, IVH rats' score on the grip test was poorer than in SHM rats (Fig. 2b), suggesting that IVH led to fine as well as gross motor impairment in the short term.

Gross motor performance was still impaired at P45 in IVH rats. Thus, coordination remained impaired and it took longer to cross the beam in IVH than in SHM rats (Fig. 2c). Motor impairment was not symmetric, with increased paresis in the contralateral forepaw as assessed using CRT (Fig. 2d). Interestingly, IVH not only resulted in motor impairment but also cognitive impairment, with IVH rats performing poorer than SHM rats in the NOR test, which reflects impaired working memory (Fig. 2e).

Long-term WMI after IVH

MRI studies at P45 revealed that IVH led to a reduction in ipsilateral forebrain hemisphere volume compared to SHM animals (Fig. 3a–c). Furthermore, CoCa area was reduced in IVH P45 rats compared to SHM rats (Fig. 3d). The volume of the lesion correlated with CoCa area reduction ($y = -5.7065x + 313.49$; $R = -0.58$, $P < 0.05$), suggesting that brain hemorrhage was related to reduction of WM volume. Accordingly, immunohistochemistry studies in the ipsilateral external capsule revealed that in IVH animals immature OL (Olig2+) cells increased at P6 with a normal density of mature OL (GSTp+). Both immature and mature OL population decreased at P14 and was severely reduced at P45, together with reduced MBP signal (Fig. 3e). In agreement, flow cytometry studies revealed that at P14 ipsilateral brain hemisphere from IVH animals showed reduced OL lineage cell density, at all developmental stages studied—O4+pre-OL, O1+ immature OL, and MOG+mature pre-myelinating OL (Fig. 6b).

BBB disruption

Gd studies did not reveal any leakage of the contrast in SHM animals at any time point. However, there was a quick leak of contrast at P6 in IVH animals, so the intensity of extravasated Gd was already increased 5 min after infusion with no further significant increase (Fig. 4). At P14, increased Gd leakage was delayed to 25 min after infusion and the final area of leakage was smaller than that observed at P6 (Fig. 4). At P45, no leakage of Gd was observed in IVH animals.

Western blot studies revealed increased expression of MMP9 and Mfsd2a in IVH compared to SHM animals at P6 and P14 (Fig. 5). Such differences were not observed at P45. No differences between groups in occludin expression were observed at any timepoint (Fig. 5).

Inflammation and other brain injury mechanisms

Excitotoxicity was assessed using ^{1}H-NMR studies, which revealed increased Glu/NAA values in IVH compared to SHM brain tissue

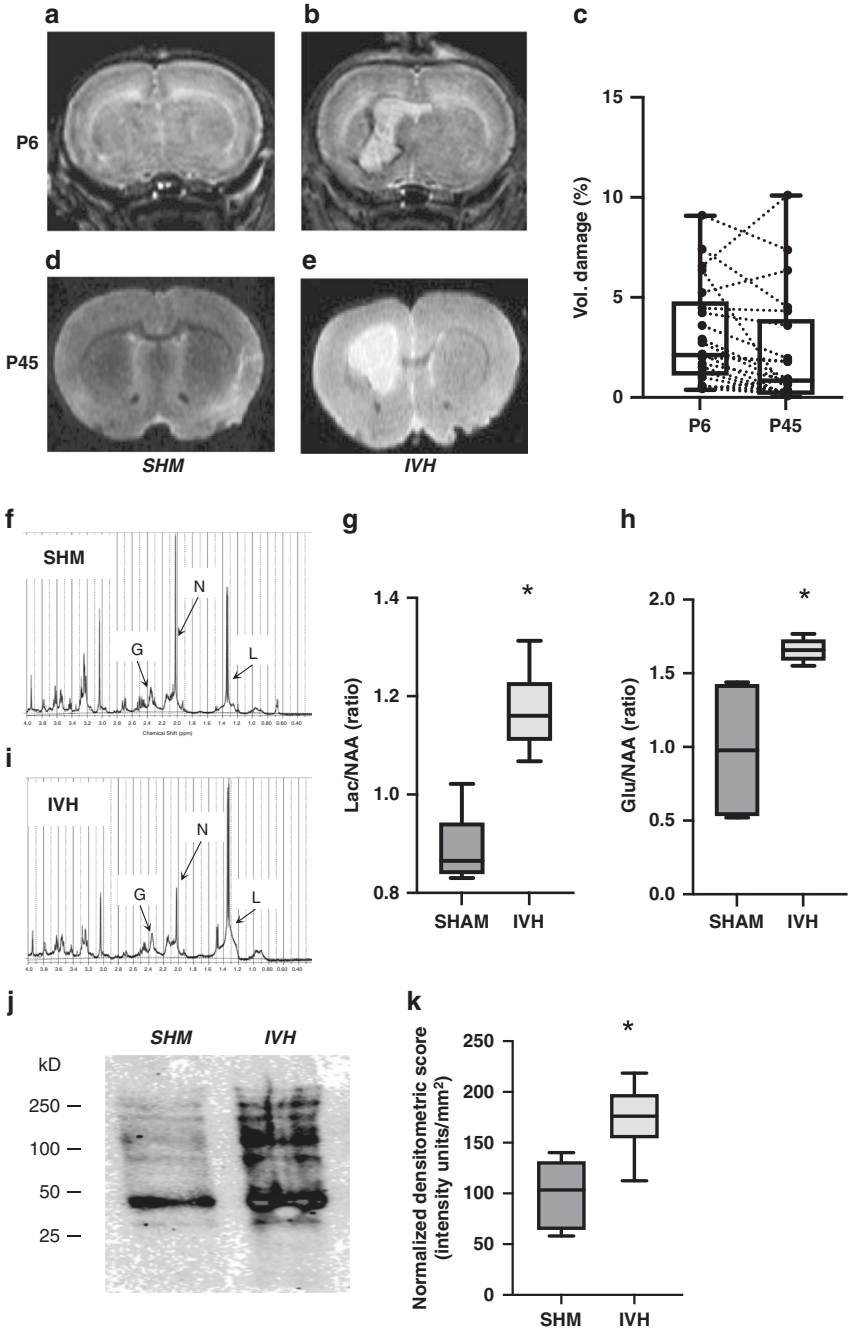

Fig. 1 Assessment of brain damage. Top, representative T2-Weighted MRI scans were obtained from SHM (**a**, **d**) and IVH (**b**, **e**) animals at P6 and P45, respectively; quantification of BD volume is shown in **c**. Middle, ^{1}H magnetic resonance studies were performed at P6 in SHM (**f**) and IVH (**i**) assessing Lac/NAA (**g**) and Glu/NAA ratio (**h**). Bottom, representative Oxyblot film (**j**) to assess at P6 protein nitrosylation (**k**). Boxes represent the median and 95% CI; whiskers represent maximum and minimum values. *$P < 0.05$ by Kruskal–Wallis test. SHM Sham, IVH intraventricular hemorrhage, Glu glutamate, Lac lactate, NAA *N*-acytylsapartate.

(Fig. 1h). IVH-induced increase in oxidative stress was analyzed using OxyBlot studies, which revealed increased protein carbonylation in the IVH brain (Fig. 1j, k).

Inflammation was studied in different ways. Western blot studies revealed that IVH was associated with increased NFκB, TLR4, and TNFα expression in the brain at P6 and P14 (Fig. 5). Differences between groups did not attain statistical significance at P45 (Fig. 5).

To further assess inflammation, the microglia population and infiltrating macrophages presented in the brain were assessed using flow cytometry studies (Fig. 6b). These revealed an increase in CD11b+/CD45^{high} (Fig. 6c) and CD11b+/CD45^{low} (Fig. 6d) populations in IVH compared to SHM, corresponding to an increased amount of activated microglia or infiltrating leukocytes and resident microglia, respectively. Such an increase was observed at P6 and P14, but at P45 no differences between SHM and IVH animals were observed. Those results corresponded with those obtained after assessing striatal Iba1+ cell density at P14 and P45 (Supplementary Material, Fig. S3). Moreover, in IVH animals a higher iNOS/Arginase ratio in CD11b+/CD45 population

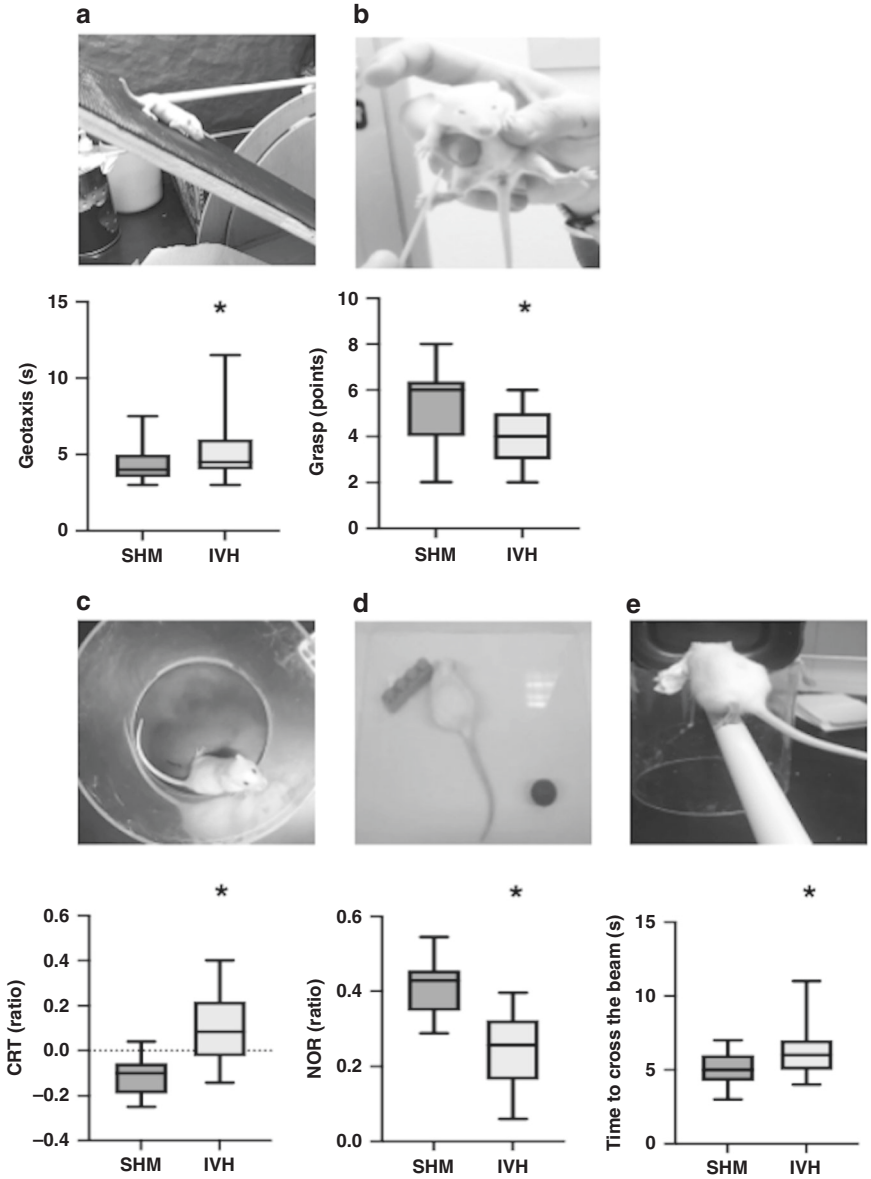

Fig. 2 Functional consequences. Neurobehavioral tests were performed at P14 (**a**, **b**) or P45 (**c**–**e**). Boxes represent the median and 95% CI; whiskers represent maximum and minimum values. *$P < 0.05$ by Kruskal–Wallis test. SHM Sham, IVH intraventricular hemorrhage, CRT cylinder rear test, NOR novel object recognition.

was observed as compared to SHM (Fig. 6e–i), corresponding to an enhanced proportion of M1 phenotype among those cells. In this case, the higher iNOS/Arginase ratio was observed only at P6.

DISCUSSION

Injecting clostridium collagenase into the GM in P1 rats led to neuroimaging, functional, and biomolecular consequences reproducing some of the hallmarks of IVH in ELBWN. These results underlie this model's strength as a tool to obtain insights into the pathophysiology of IVH-induced brain damage in ELBWN. The developmental stage at P1 is similar to 24–25 weeks.[16] This is a remarkable difference that respects previous PVCC models since extremely preterm newborns have a higher incidence and severity of IVH and IVH-induced brain damage.[1,2]

IVH induced by PVCC leads to periventricular brain damage demonstrated five days after IVH induction by histologic assessment, accordingly to previous studies in P2[17] and P7 rats.[11] At the same time point, i.e., P6, MRI studies revealed in that area an increased intensity signal together with increased Lac/NAA ratio, a surrogate of brain damage.[22] Brain injury after IVH is due to ischemia induced by the mass effect of blood hematoma, followed by the toxic effect of different components of extravasated blood.[4,6] The periventricular area in the immature brain has a high presence of OL lineage cells,[6] in particular immature OL[25] which are the cells most vulnerable to brain damage.[26] Thus, WMI is a prevalent condition in ELBWN surviving brain injury and presenting developmental disturbances[27] which results in long-term reduction of brain volume[28] as well as CoCa volume,[29] as assessed by MRI studies. Those features were reproduced in our model, with reduced ipsilateral hemisphere volume and CoCa area observed in MRI studies at P45 in IVH rats. Those MRI features, not reported in PVCC models in P7 rats, were associated with WMI. At P6, an increased density of Olig2+ cells was observed, in agreement with the increased density of NG2+ cells reported in P2 rats 6 days after PVCC.[17] Then, both immature and mature OL population decreased to result severely reduced at P45, together with reduced MBP signal. Since at P1 in Wistar rat brain almost all

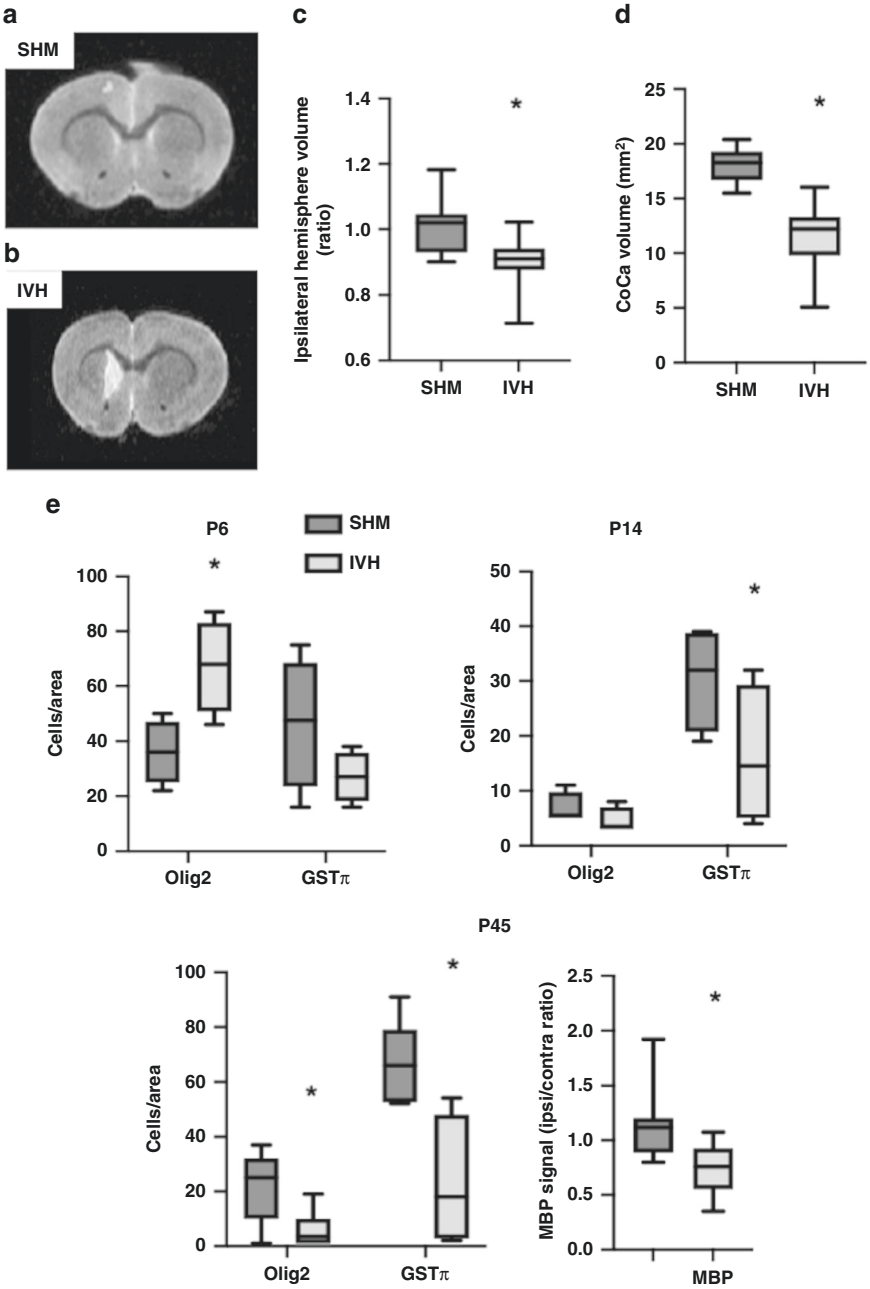

Fig. 3 White matter injury. Top, representative T2-weighted MRI scans were obtained from SHM (Sham; **a**) and IVH (intraventricular hemorrhage; **b**) animals at P45, to determine ipsilateral hemisphere (**c**) and corpus callosum (CoCa) (**d**) atrophy. Bottom **e**, graphical representation of immunohistochemistry studies assessing in the ipsilateral external capsule immature (Olig2) and mature (GSTπ) oligodendroglial population at P6, P14, and P45 as well as myelin basic protein (MBP) signal at P45. Boxes represent the median and 95% CI; whiskers represent maximum and minimum values. *$P < 0.05$ by Kruskal–Wallis test vs. SHM.

the OL population is comprised of pre-OL,[25,30] those results suggest that, despite the initial proliferative response of immature OL, IVH was not only inducing immature OL death but also impairing their maturational processes.[6] A similar picture is described in other very immature brain damage models.[30] GM plays a critical role in the production of OL precursors,[31] a process jeopardized by IVH affecting the GM.[32] IVH-induced hypomyelination has not been reported for PVCC models in P7 rats.

Since WMI is a major cause of developing CP in ELBWN we explored whether IVH was associated with long-lasting functional deficits. IVH rats showed motor disturbances with impaired negative geotaxis and grip test performance at P14 and increased time to cross a beam at P45, as well as some cognitive impairment with impaired working memory at P45. Those deficits correspond to those reported in PVCC models in P7 rats.[11] Interestingly, in our model it was also revealed that IVH rats have long-term strength impairment with worse CRT performance at P45, a finding not reported previously in PVCC models in P7 rats.

BBB disruption plays a key role in intracerebral hemorrhage-induced BD in mature[33] and immature[6] brain. Aside from confirming that IVH induced BBB increased permeability we also reported the time course of this abnormality. Increased BBB permeability, as shown by increased Gd leakage assessed by MRI, was remarkable five days after IVH induction, a feature that coincides with the increased tracer leakage observed 24 and 72 h after PVCC in P5 and P7 rats, respectively.[14,15] Interestingly, Gd

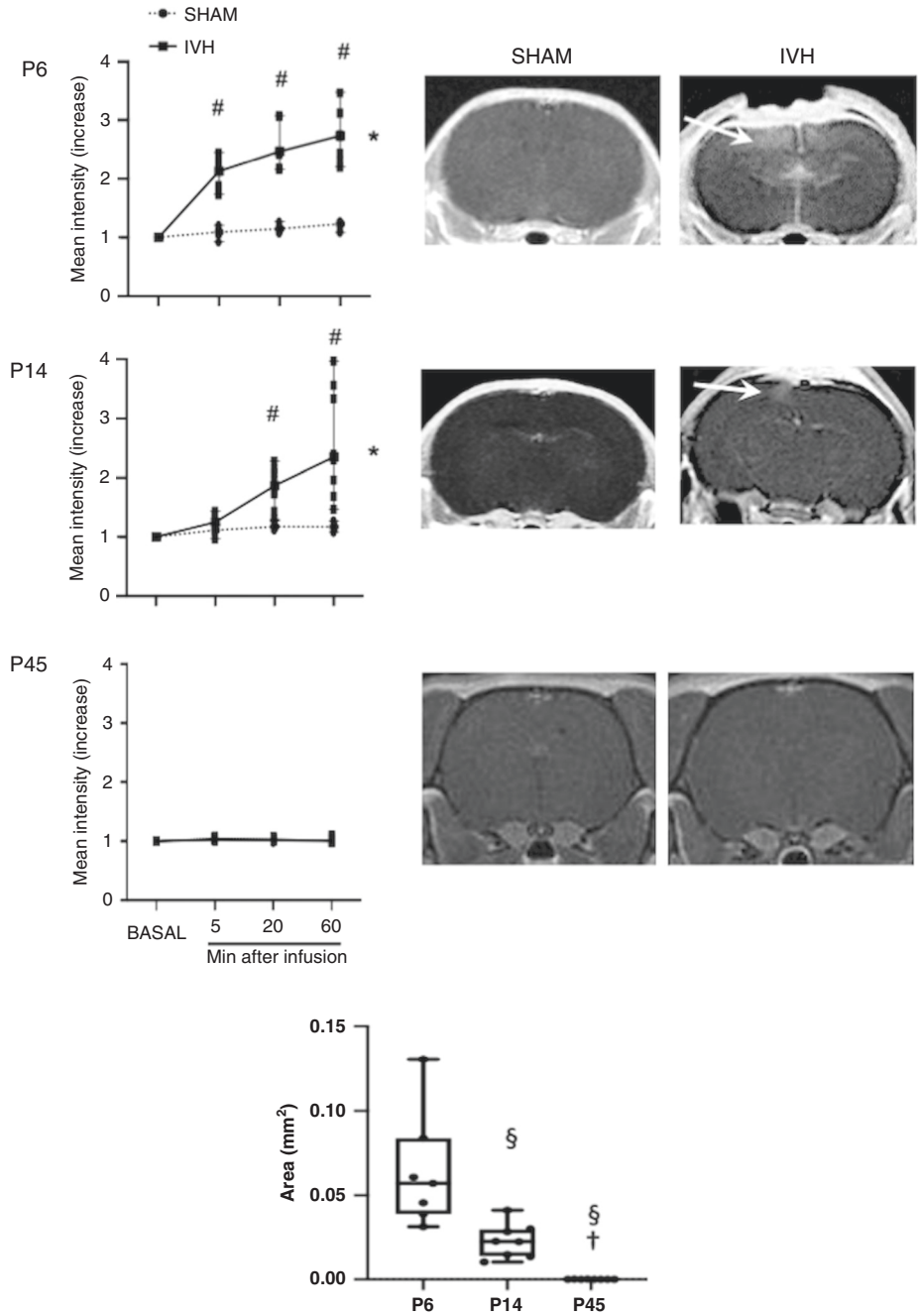

Fig. 4 Increased blood–brain barrier (BBB) permeability. Top, the intensity of gadolinium signal at P6, P14, and P45 in T1W MRI just before and 5, 20, and 60 min after infusion; representative MRI scans were obtained 60 min post-infusion. Arrows point to the increased intensity area reflecting gadolinium leakage. Bottom, determination of the area of gadolinium leakage 60 min post-infusion at P6, P14, and P45. Boxes represent the median and 95% CI; whiskers represent maximum and minimum values. SHM Sham, IVH intraventricular hemorrhage. $^{\#}P < 0.05$ by 2-way ANOVA. $^{\S}P < 0.05$ vs. P6 and $^{\dagger}P < 0.05$ vs. P14 by Kruskal–Wallis with Dunn's post hoc test for multiple comparison.

leakage was still observable at P14. BBB permeability, assessed by radio-tagged sucrose leakage measured ex vivo in brain slices from P5 rats was no longer observed 5 days after PVCC.[15] The difference with our results may be due to developmental differences in BBB responses in P1 and P5 rats but may also indicate a higher sensitivity for real-time in vivo assessment of BBB permeability using MRI after Gd infusion. BBB permeability has two main determinants, the paracellular and the transcellular routes. We assessed these by determining the expression of occludin (a component of tight junctions) and Mfsd2a (a vesicular transcytosis regulator), respectively.[33,34] We did not detect any variation in occludin expression from four days after IVH. However, occludin expression is reduced 72 h after PVCC in P7 rats.[14] This suggests that the more immature the brain the greater the resistance of tight junctions to IVH-induced brain insult. It also highlights the importance of selecting a specific postnatal age when performing translational models of immature brain damage. By contrast, we observed a decrease in Mfsd2a expression, which is associated with increased BBB permeability due to reduced modulation of vesicular transcytosis in adult rats after intracerebral hemorrhage.[33] Decreased Mfsd2a expression was observed at P6 and P14 but not at P45, which is at the same time points as

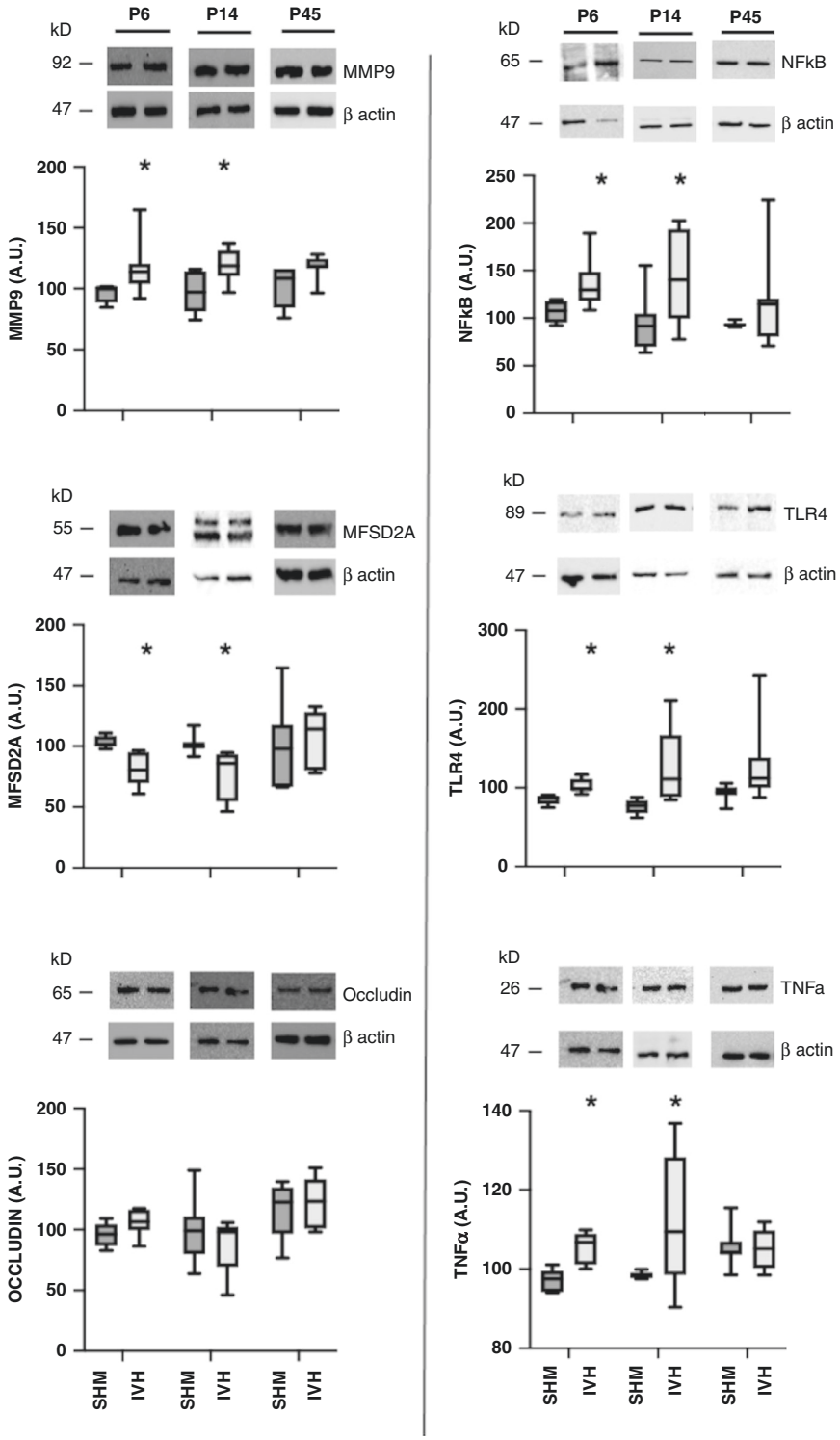

Fig. 5 Modification of the expression of biomarkers related to brain–blood barrier and neuroinflammation. Representative samples of western blot studies performed in brain samples obtained from SHM (Sham) and IVH (intraventricular hemorrhage) animals at P6, P14, and P45 and the corresponding graphical representation of the densitometric analysis. Boxes represent the median and 95% CI; whiskers represent maximum and minimum values. *$P < 0.05$ Kruskal–Wallis test. Mfsd2a major facilitator superfamily domain-containing protein 2A, MMP9 metallopeptidase 9, NFκB nuclear factor κ B, TLR4 toll-like receptor 4, TNFα tumor necrosis factor α.

increased Gd leakage. This supports a relationship between Mfsd2a decrease and increased BBB permeability. Moreover, it suggests that IVH led to BBB dysfunction rather than BBB disruption.

Mechanisms of IVH-induced brain damage are not fully understood. However, it is known that blood extravasation in GM triggers a strong inflammatory response due to brain infiltration by inflammatory cells and the effect of Hb released after

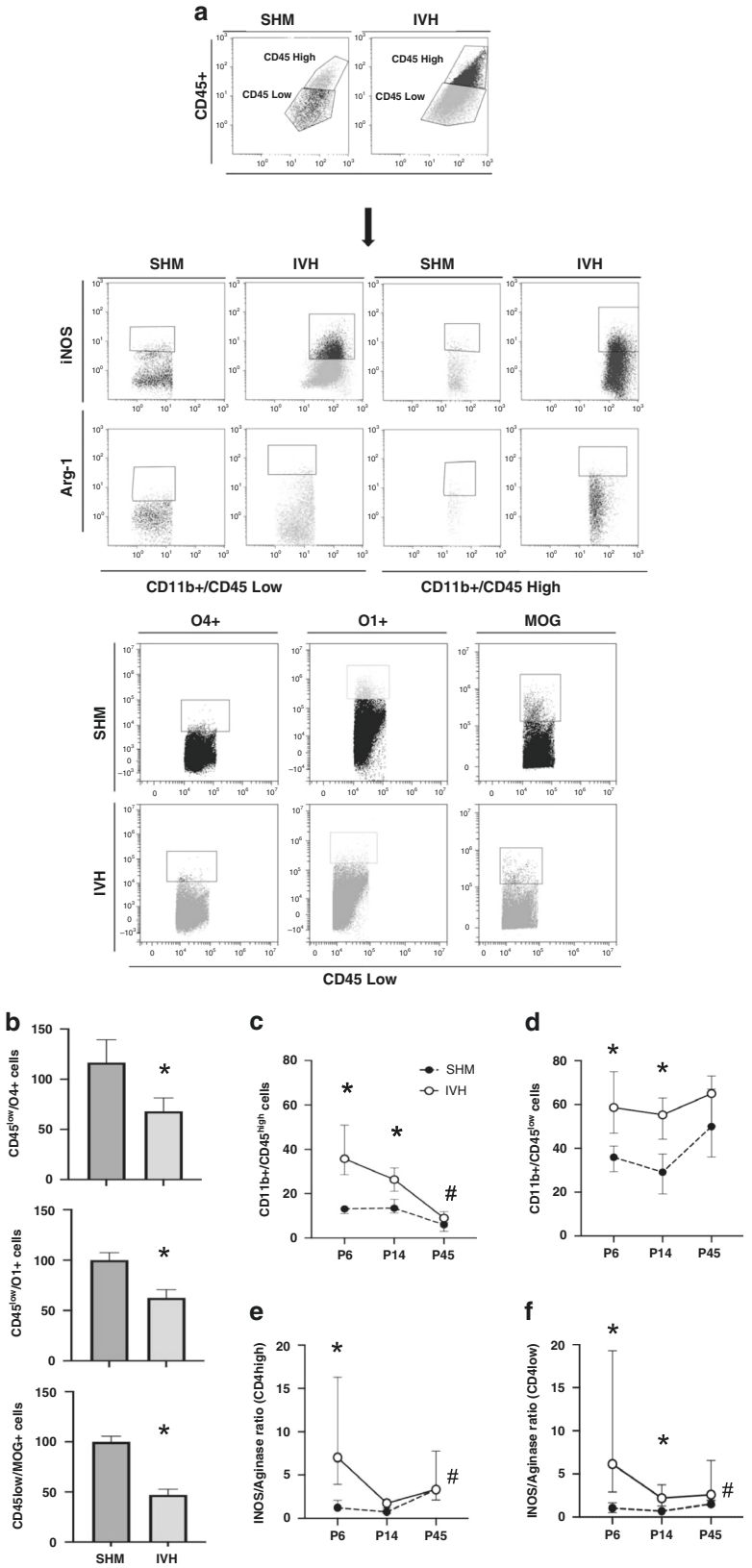

Fig. 6 Flow cytometry studies. a Representative plots from flow cytometry performed in brain samples from SHM (sham) and IVH (intraventricular hemorrhage) animals. **b** To identify cells from oligodendroglial lineage at P14 at different maturational stages, $CD45^{low}$ cells were labeled with O4, O1, or MOG antibodies. Bars represent the mean (SEM). $^{*}P < 0.05$ by two-tailed *t* test. To study microglia/macrophages at P6, P14, and P45, cells were labeled with CD11b and CD45 antibodies to identify **c** CD11b+/$CD45^{high}$ and **d** CD11b+/$CD45^{low}$ population as well as the iNOS/Arginase ratio in $CD45^{high}$ (**e**) and $CD4^{low}$ (**f**) cells. Lines represent the mean (95% CI). $^{*}P < 0.05$ vs. SHM at each timepoint, $^{\#}P < 0.05$ by 2-way ANOVA.

hemolysis.[1] Inflammation leads to increased excitotoxicity in addition to oxidative stress.[33,35,36] Those key factors are of paramount importance for WMI in the immature brain because immature OL is extremely vulnerable to their effects.[26,37] In our study, IVH led to increased inflammatory cellularity in periventricular brain tissue at P6 and P14, with increased density of CD11b+/CD45^{high} cells, which corresponds to infiltrating neutrophils and macrophages as well as activated microglia.[23] These play a key role in neuroinflammation.[37] Microglial phenotypes are usually reported as M1 (iNOS+, with pro-inflammatory properties) and M2 (Arginase+, with restorative properties).[23,24] In adult rodents, shortly after the induction of intracerebral hemorrhage the proportion of M1 is dramatically increased over that of the M2 phenotype.[38] Such an imbalance, as shown by the increased iNOS/arginase ratio we observed in IVH animals, is related to inflammatory brain injury.[24] In adult mice models, intracerebral hemorrhage upregulates the expression of TLR4 in activated microglia, which is an important mechanism of inflammation-mediated brain injury.[36] Moreover, extravasated blood upregulates TLR4 expression in brain tissue.[36] We have demonstrated that IVH also led to TLR4 upregulation in the immature brain. In addition to activating different damaging inflammatory pathways, TLR4 activation leads to increased oxidative stress and excitotoxicity.[33,35,36] Accordingly, after IVH we observed in brain tissue increased protein nitrosylation, a marker of oxidative stress seen after acute injury in the immature brain.[21,22] We also observed increased excitotoxicity in the IVH brain with an increased Glu/NAA ratio. Excitotoxicity could be particularly harmful in this scenario since TLR4 activation upregulates NMDA signaling.[35] The parallel between increased Gd leakage and increased density of CD11b+/CD45^{high} cells supports the notion that increased BBB permeability was a key factor for IVH-induced infiltration of immune cells and vice versa.[37] Therefore, we detected increased levels of TNFα at P6 and P14 but not at P45 in IVH animals. Enhanced inflammation in the brain prompts increased MMP9 production by means of NFkB activation. In turn, MMP9 enhances the inflammatory response.[39,40] In accordance with this, we observed increased MMP9 expression in parallel to that of TNFα and NFκB in IVH animals, although NFκB results should be taken with caution since we did not measure NFκB activity. Increased MMP9 production is associated with WMI and increased BBB permeability.[39,40] MMP9 affects BBB permeability by damaging tight junctions but also by inducing pericyte dysfunction.[39–41] The latter is probably the more relevant mechanism of MMP9-induced increased BBB permeability in our study considering that occludin levels were unchanged after IVH. Again, MMP9 results should be taken with caution since we did not measure MMP9 activity. Gd leakage outside the boundaries of the area surrounding PVCC is also observed in P5 rats 24 h after PVCC.[15]

Our work presents several shortcomings. Although ventriculomegaly is a typical consequence of IVH in this model,[11] we were unable to determine such complication separately because we included all hyperintense and hypointense areas in measurements at T2WI studies. intracerebral collagenase injection can exaggerate by itself the inflammatory response.[10,42] However, that effect is observed after PVCC to adult rats and at a dose higher (0.4–2 U)[10,42] than that used in our study (0.2 U). In fact, the dose of collagenase used in our study was lower than those usually reported for neonatal models of PVCC,[11,14,15,17] which is relevant because collagenase effects are dose-dependent.[12] Besides, inflammatory effects of collagenase peak 3 days after injection,[12,42] whereas in our model increased inflammation and BBB disruption were still observable 13 days after injection.

In conclusion, injection of PVCC into P1 rats reproduced some of the neuroimaging, functional and pathophysiologic features characteristic of IVH in ELBWN and its consequences. Our data suggest that blood extravasated into the periventricular parenchyma after IVH triggers a prolonged inflammatory response associated with BBB increased permeability, which in turn facilitates the infiltration of inflammatory cells. Such processes eventually lead to WMI, which results in long-lasting motor and cognitive deficits. This model offers some clues to obtain further insight into the mechanisms of BD in ELBWN, which can be helpful for the development of therapeutic strategies to alleviate the devastating consequences of a prevalent condition currently orphan from effective treatments.

DATA AVAILABILITY

The datasets generated during and/or analyzed during the current study are available from the corresponding author on reasonable request.

REFERENCES

1. Ballabh, P. Pathogenesis and prevention of intraventricular hemorrhage. *Clin. Perinatol.* **41**, 47–67 (2014).
2. Brouwer, M. J. et al. Effects of posthemorrhagic ventricular dilatation in the preterm infant on brain volumes and white matter diffusion variables at term-equivalent age. *J. Pediatr.* **168**, 41–49 (2016).
3. Bolisetty, S. et al. Intraventricular hemorrhage and neurodevelopmental outcomes in extreme preterm infants. *Pediatrics* **133**, 55–62 (2014).
4. Garton, T., Hua, Y., Xiang, J., Xi, G. & Keep, R. F. Challenges for intraventricular hemorrhage research and emerging therapeutic targets. *Expert Opin. Ther. Targets* **21**, 1111–1122 (2017).
5. Zhao, X. et al. Distinct patterns of intracerebral hemorrhage-induced alterations in NF-κB subunit, iNOS, and COX-2 expression. *J. Neurochem.* **101**, 652–663 (2007).
6. Romantsik, O., Bruschettini, M. & Ley, D. Intraventricular hemorrhage and white matter injury in preclinical and clinical studies. *Neoreviews* **20**, 636–652 (2019).
7. Linsell, L., Malouf, R., Morris, J., Kurinczuk, J. J. & Marlow, N. Prognostic factors for cerebral palsy and motor impairment in children born very preterm or very low birthweight: a systematic review. *Dev. Med. Child Neurol.* **58**, 554–569 (2016).
8. Fowlie, P. W., Davis, P. G. & McGuire, W. Prophylactic intravenous indomethacin for preventing mortality and morbidity in preterm infants. *Cochrane Database Syst. Rev.* CD000174 (2010).
9. Balasubramaniam, J. & Del Bigio, M. R. Animal models of germinal matrix hemorrhage. *J. Child Neurol.* **21**, 365–371 (2006).
10. Alles, Y. C. J. et al. A novel preclinical rodent model of collagenase-induced germinal matrix/intraventricular hemorrhage. *Brain Res.* **1356**, 130–138 (2010).
11. Lekic, T. et al. Rodent neonatal germinal matrix hemorrhage mimics the human brain injury, neurological consequences, and post-hemorrhagic hydrocephalus. *Exp. Neurol.* **236**, 69–78 (2012).
12. Manaenko, A., Chen, H., Zhang, J. H. & Tang, J. Comparison of different preclinical models of intracerebral hemorrhage. *Acta Neurochir. Suppl.* **111**, 9–14 (2011).
13. Segado-Arenas, A. et al. Cognitive impairment and brain and peripheral alterations in a murine model of intraventricular hemorrhage in the preterm newborn. *Mol. Neurobiol.* **55**, 4896–4910 (2018).
14. Rolland, W. B. et al. Fingolimod confers neuroprotection through activation of Rac1 after experimental germinal matrix hemorrhage in rat pups. *J. Neurochem.* **140**, 776–786 (2017).
15. Andersson, E. A., Rocha-ferreira, E., Hagberg, H., Mallard, C. & Ek, C. J. Function and biomarkers of the blood-brain barrier in a neonatal germinal matrix haemorrhage model. *Cells* **10**, 1677 (2021).
16. Semple, B. D., Blomgren, K., Gimlin, K., Ferriero, D. M. & Noble-Haeusslein, L. J. Brain development in rodents and humans: Identifying benchmarks of maturation and vulnerability to injury across species. *Prog. Neurobiol.* **106–107**, 1–16 (2013).
17. Martins, C. A. et al. Neuroprotective effect of ACTH on collagenase-induced peri-intraventricular hemorrhage in newborn male rats. *Sci. Rep.* **10**, 17734 (2020).
18. Paxinos, G. & Watson, C. *The Rat Brain in Stereotaxic Coordinates* 3rd edn (Academic Press, 1997).
19. Ceprián, M. et al. Cannabidiol reduces brain damage and improves functional recovery in a neonatal rat model of arterial ischemic stroke. *Neuropharmacology* **116**, 151–159 (2017).
20. Ceprián, M. et al. Cannabidiol administration prevents hypoxia-ischemia-induced hypomyelination in newborn rats. *Front. Pharmacol.* **10**, 1131 (2019).
21. Pazos, M. R. et al. Mechanisms of cannabidiol neuroprotection in hypoxic-ischemic newborn pigs: role of 5HT(1A) and CB2 receptors. *Neuropharmacology* **71**, 282–291 (2013).
22. Barata, L. et al. Neuroprotection by cannabidiol and hypothermia in a piglet model of newborn hypoxic-ischemic brain damage. *Neuropharmacology* **146**, 1–11 (2019).

23. Truettner, J. S., Bramlett, H. M. & Dietrich, W. D. Posttraumatic therapeutic hypothermia alters microglial and macrophage polarization toward a beneficial phenotype. *J. Cereb. Blood Flow Metab.* **37**, 2952–2962 (2017).
24. Mecha, M., Carrillo-Salinas, F. J., Feliú, A., Mestre, L. & Guaza, C. Microglia activation states and cannabinoid system: therapeutic implications. *Pharmacol. Ther.* **166**, 40–55 (2016).
25. Dean, J. M. et al. Strain-specific differences in perinatal rodent oligodendrocyte lineage progression and its correlation with human. *Dev. Neurosci.* **33**, 251–260 (2011).
26. Volpe, J. J. The encephalopathy of prematurity-brain injury and impaired brain development inextricably intertwined. *Semin. Pediatr. Neurol.* **16**, 167–178 (2009).
27. Newville, J., Jantzie, L. & Cunningham, L. Embracing oligodendrocyte diversity in the context of perinatal injury. *Neural Regen. Res.* **12**, 1575 (2017).
28. Dorner, R. A., Burton, V. J., Allen, M. C., Robinson, S. & Soares, B. P. Preterm neuroimaging and neurodevelopmental outcome: a focus on intraventricular hemorrhage, post-hemorrhagic hydrocephalus, and associated brain injury. *J. Perinatol.* **38**, 1431–1443 (2018).
29. Thompson, D. K. et al. Corpus callosum alterations in very preterm infants: perinatal correlates and 2year neurodevelopmental outcomes. *Neuroimage* **59**, 3571–3581 (2012).
30. Segovia, K. N. et al. Arrested oligodendrocyte lineage maturation in chronic perinatal white matter injury. *Ann. Neurol.* **63**, 520–530 (2008).
31. Kriegstein, A. & Alvarez-Buylla, A. The glial nature of embryonic and adult neural stem cells. *Annu. Rev. Neurosci.* **32**, 149–184 (2009).
32. Choi, E.-K. et al. Animal models of periventricular leukomalacia. *Lab. Anim. Res.* **27**, 77–84 (2011).
33. Yang, Y.-R. et al. Mfsd2a (major facilitator superfamily domain containing 2a) attenuates intracerebral hemorrhage-induced blood-brain barrier disruption by inhibiting vesicular transcytosis. *J. Am. Heart Assoc.* **6**, e005811 (2017).
34. Saunders, N. R., Dziegielewska, K. M., Møllgård, K. & Habgood, M. D. Physiology and molecular biology of barrier mechanisms in the fetal and neonatal brain. *J. Physiol.* **596**, 5723–5756 (2018).
35. Zimmer, J., Kristensen, B. W., Jakobsen, B. & Noraberg, J. Excitatory amino acid neurotoxicity and modulation of glutamate receptor expression in organotypic brain slice cultures. *Amino Acids* **19**, 7–21 (2000).
36. Lin, S. et al. Heme activates TLR4-mediated inflammatory injury via MyD88/TRIF signaling pathway in intracerebral hemorrhage. *J. Neuroinflammation* **9**, 548 (2012).
37. Bhalala, U. S., Koehler, R. C. & Kannan, S. Neuroinflammation and neuroimmune dysregulation after acute hypoxic-ischemic injury of developing brain. *Front. Pediatr.* **2**, 1–12 (2015).
38. Zhao, H., Garton, T., Keep, R. F., Hua, Y. & Xi, G. Microglia/macrophage polarization after experimental intracerebral hemorrhage. *Transl. Stroke Res.* **6**, 407–409 (2015).
39. Rempe, R. G. Matrix metalloproteinases in the brain and blood–brain barrier: versatile breakers and makers. *J. Cereb. Blood Flow Metab.* **36**, 1481–1507 (2016).
40. Svedin, P., Hagberg, H., Sävman, K., Zhu, C. & Mallard, C. Matrix metalloproteinase-9 gene knock-out protects the immature brain after cerebral hypoxia-ischemia. *J. Neurosci.* **27**, 1511–1518 (2007).
41. Qin, W. et al. Melatonin protects blood-brain barrier integrity and permeability by inhibiting matrix metalloproteinase-9 via the NOTCH3/NF-kB pathway. *Aging* **11**, 11391–11415 (2019).
42. Xue, M. & Del Bigio, M. R. Comparison of brain cell death and inflammatory reaction in three models of intracerebral hemorrhage in adult rats. *J. Stroke Cerebrovasc. Dis.* **12**, 152–159 (2003).

ACKNOWLEDGEMENTS

We thank the Flow Cytometry Unit of Hospital Clinico San Carlos-IdISSC for excellent technical assistance and Jason Willis-Lee MITI for medical writing assistance.

AUTHOR CONTRIBUTIONS

A.D.P.: conceptualization, methodology, investigation, data curation, writing—original draft. M.V., C.V., D.C.: investigation, data curation. E.F.-V.: conceptualization, investigation, resources. A.G.-R.: conceptualization, methodology, investigation, writing—original draft. J.M.-O.: conceptualization, methodology, formal analysis, resources, writing—original draft, writing—review and editing.

FUNDING INFORMATION

This work was supported by the PI19/00927 project, integrated into the Plan National de I + D + I, AES 2017-2020; funded by the ISCIII and co-funded by the European Regional Development Fund (ERDF) "A way to make Europe."

COMPETING INTERESTS

The authors declare no competing interests.

CONSENT FOR PUBLICATION

Not applicable.

ADDITIONAL INFORMATION

Supplementary information The online version contains supplementary material available at https://doi.org/10.1038/s41390-022-02062-3.

Correspondence and requests for materials should be addressed to José. Martínez-Orgado.